Extended abstract proposed for
AIAA/CEAS Aeroacoustics Conference
June 4-7, 2024
Rome, Italy

Area: Jet Aeroacoustics

Study of a plug nozzle for supersonic aircraft concepts

Khairul B.M.Q. Zaman[1], John H. Korth[2], Amy F. Fagan[3] and James, E. Bridges[4]
NASA Glenn Research Center
Cleveland, OH 44135

1. Introduction

Nozzles with external plugs are candidates for the exhaust system of supersonic aircraft concepts in an ongoing research effort at NASA. As part of that effort a fundamental study is being conducted at NASA Glenn Research Center (GRC). Experimental and limited numerical simulation results from this study, for a plug nozzle with a convergent nozzle (cowl), have been reported in recent publications [1, 2]. Conventional method-of-characteristics (MoC) design for the plug requires that the flow is choked at the nozzle exit. This is why a sharp convergence of the cowl is invoked in such a design in most previous studies [3-5], leading to the earlier choice of the convergent cowl. Such a nozzle, however, is not suitable for supersonic flights because of large boattail drag suffered by its outer surface. The boattail drag consideration dictates that the cowl be more or less cylindrical in shape. While various other shapes have been studied in the past [6], essentially a cylindrical shape is adopted in the larger research program at NASA. The cylindrical shape has certain advantages. With the plug crown located somewhat inside the nozzle, the flow experiences convergence and divergence as with a C-D nozzle. By translating the plug, different throat-to-exit area ratio could be achieved to obtain fully expanded condition at different values of NPR. This offers a relatively easy active control strategy for the nozzle geometry throughout the flight regime from landing and takeoff (LTO) to cruise conditions.

A plug nozzle model mimicking the geometry being considered in the NASA program, i.e., having a cylindrical exit, have been fabricated recently for continued fundamental studies. Some of the plugs used with the earlier convergent cowl [1] are readily adopted to this model. In addition, a few other plugs have been obtained following a numerical optimization study [7]. The various configurations are to be investigated for thrust, noise and flow fields, with complementing numerical simulations. Thrust data for a variety of configurations as well as limited noise data are in hand. Further explorations including schlieren visualization are to be conducted in the near future. The proposed paper is to summarize all these results. In the following, a few key results obtained so far are described.

[1] Inlets & Nozzles Branch, AIAA Associate Fellow.
[2] Inlets & Nozzles Branch, AIAA Member.
[3] Optics & Photonics Branch, AIAA Associate Fellow.
[4] Acoustics Branch, AIAA Associate Fellow.

2. Experimental Facility and Procedure

2.1 Jet facility and plug nozzle geometries:

The experiments are conducted in an open jet facility at GRC [1, 2]. The thrust measurement setup is shown in Fig. 1(a). Flow from a fixed upstream plenum (attached to the end of the facility) is routed through four U-shaped pipes (i.d. = 1.31 in.) to enter radially into a 'floating' plenum chamber. The latter is mounted on a linear bearing allowing it to move freely in the axial direction. The four U-shaped feed tubes each has a flexible component. The flow from the 5" diameter floating plenum passes through two 30-mesh screens and then exhausts through the nozzle. The axial force is measured by a load cell attached to the face of the fixed plenum chamber. However, inertia, friction etc. come into play and the data reduction for actual thrust from the measured force is not straightforward. Convergent (ASME) nozzles are used for calibration of the apparatus.

The plug nozzle is attached to the end of the floating plenum chamber (Fig. 1b). The nozzle has 2" exit diameter. All dimensions are given in inches. There is a fixed 0.75" diameter cylindrical part held centrally within the nozzle by X-shaped struts. A lead screw fixed to the cylindrical part is used to attach the interchangeable plugs. Spacers placed at the junction between the plug and the cylindrical part allow for variation of the axial location of the plug crown. The cylindrical section near the exit of the nozzle can be extended using extension pieces shown in Fig. 1(c). These simply fit over the end of the nozzle. Extensions E1, E2, E3 and E4 extend the lip location by 0", 0.38", 0.74" and 1.34".

A few plugs used in the experiment are shown in Figs. 1(d-g). Three conic plugs with half angles of 10°, 16° and 22° (denoted as 'P10P', 'P16P' and 'P22P') are shown in Fig. 1(d). While the plugs in Fig. 1(d) are solid, corresponding porous plugs ('PRS6', 'PRS2' and 'PRS7') are shown in Fig. 1(e). A porous plug has identical external geometry as its solid counterpart but has an internal cavity. The cavity has four quadrants separated by X-shaped struts to support the skin with pores. Details of the 10° conic porous plug (PRS6) is shown by the CAD drawings in Fig. 1(f). The 'openness ratio', i.e., the ratio of open area due to the pores to the total surface area of the skin is 6% for all porous plugs considered in this abstract.

The three plugs shown in Fig. 1(g) were designed following a numerical optimization study [7]. The plug geometry was varied by varying three parameters, L_{t1}, L and P, as shown in Fig. 2(a). By varying these parameters, a wide range of plug geometries could be obtained. Numerical simulation provided thrust coefficient for each geometry for varying NPR. A design space was queried to determine the geometry yielding optimum thrust at a chosen flight condition (NPR). This way, two optimum geometries were obtained for LTO and cruise conditions. These two are P38 and P39 in Fig. 2(b) (referred to as K1b and K7 in [7]). Thus, P38 has best CFG at LTO condition (NPR≈2) but lower CFG at cruise (NPR≈5.9), and vice versa for P39. The third geometry (P40; referred to as K9 in [7]) is a 'compromise' case yielding good CFG over the entire NPR range. Plugs of these three geometries were fabricated, and shown in Fig. 1(g), for experimental studies.

Overhead microphones were used to measure radiated noise. Noise data presented in this abstract pertain to a microphone location of 90° to the jet axis, on the nozzle exit plane. The microphone data acquisition is done using National Instruments A/D card and Labview™ software. Sound pressure level spectral analysis is done typically over 0-50kHz with a bandwidth of 50 Hz, using a data rate of 100 kHz and a 50 kHz low-pass filter. The 'jet Mach number' M_J is defined based on the plenum pressure, p_0, and the ambient pressure, p_a, and given by, $M_J = (((p_0/p_a)^{(\gamma-1)/\gamma} - 1)\frac{2}{\gamma-1})^{1/2}$, where γ is the ratio of specific heats for air, the nozzle pressure ratio NPR being equal to p_0/p_a. All data are for unheated flow, i.e., with the total temperature the same everywhere as in the ambient.

2.2 Data reduction for CFG:

As stated before, finding thrust from the measured axial force was not straightforward. The thrust rig performance was examined using convergent nozzles of different diameters. These nozzles have internal contours similar to standard ASME nozzles. The measured axial force (Tm) and mass flow rate (mdot), for three such nozzles with exit diameters of 1.1", 1.3" and 1.5", are shown in Fig. 3(a) and (b) as a function of NPR. The mdot data are obtained by an orifice-meter in the supply line. The Tm data are compared in Fig. 4(a) with the expected actual thrust (Tac). Tac is calculated as follows. The ideal thrust T_{ideal} is calculated first. This is simply a function of NPR and independent of temperature [8]. It assumes uniform flow with zero boundary layer thickness. In the supersonic regime it represents the thrust had the flow expanded fully. Then a correlation for thrust coefficient (CT) for ASME nozzles, based on a large set of data from different sources [9], is used to determine Tac=T_{ideal}*CT. The force Tac would be measured had the thrust rig responded correctly without any friction or inertia. As it can be seen in Fig. 4(a) the measured force Tm differs from Tac.

The friction and binding forces due to tautness of the feed tubes under pressure ('tare' force) was measured by capping the nozzle while varying the plenum pressure. The Tare data are also shown in Fig. 4(a). The expectation was that a correction with Tare would directly yield the actual thrust, i.e., Tac = Tm+Tare. However, for all conditions the measured Tare was not adequate to account for the difference between Tm and Tac. Furthermore, there was a noticeable hysteresis in Tare. Efforts were made to eliminate the hysteresis, without success. At this point, the idea of measuring thrust directly was abandoned and a method was adopted based on calibration data from the ASME nozzles.

The method involved recording the difference Tac-Tm as a function of NPR for the three ASME nozzles, as shown in Fig. 4(b). Now, for a plug nozzle Tm and mdot were measured as a function of NPR. For a given NPR, the mdot data was used to find an equivalent diameter (D_{eq}) by interpolation of the calibration data of Fig. 3(b). The value of Tac-Tm, for that D_{eq} and NPR, was then found from Fig. 4(b), that yielded the expected actual thrust Tac. Calculated ideal thrust provided the gross thrust coefficient CFG (=Tac/ T_{ideal}). The uncertainty in the CFG data obtained over a period of weeks is found to be large. However, it is small enough for data obtained back-to-back to allow an assessment of comparative performance with parametric variations. The uncertainty in CFG (standard deviation) for several sets of data for the 1.3" ASME nozzle, acquired over a day, was determined to be 0.45% and 0.7% for NPR of 4.2 and 2, respectively.

3. Preliminary Results

Thrust coefficient for the three optimized plugs, P38, P39 and P40 are shown in Fig. 5 as a function of NPR. The plug crown location was fixed at △x= -0.035". Even though in the optimization △x was different for each NPR (to obtain fully expanded flow), the three plug cases in Fig. 5 have yielded trends as expected. At low NPR, the LTO optimized case (P38, blue line) produced high CFG while the cruise optimized case (P39, red line) has low CFG, and vice versa at the high end of the NPR range. The compromise case (P40, green curve) has intermediate performance at high NPR whereas it is seen to perform quite well at low NPR.

The performance of the P40 plug was examined as the crown location was varied. Corresponding CFG data are shown in Fig. 6. When the crown is located just downstream of the nozzle exit (△x=+0.028"), the performance is poor (red solid curve). As the crown is drawn inside the performance improves. With △x=-0.665", largest CFG is obtained on the right end of the figure (as cruise condition is approached). With further decrease in △x the performance degrades.

The plug porosity effect is illustrated in Fig. 7, with data from two solid conic plugs (P10 and P16) and their porous counterparts (PRS6 and PRS2). While a reduction in CFG, due to porosity, in the order of 1% is noted for the 16° case (Fig. 7b), a smaller reduction over most of the NPR range is noted for the 10° case (Fig. 7a). The results delineate that the losses in CFG with the presently used porous plugs are quite small. Preliminary data showed that the noise reductions by some of the porous plugs, on the other hand, are quite significant. The noise reduction vis-à-vis thrust loss by the porous plugs will be examined further and the results summarized in the final paper.

Some of the parametric variations were investigated through Computational Fluid Dynamics (CFD) analysis. First, as a sanity check CFG for the *D*=1.3" ASME nozzle is examined. Numerical and experimental data are presented in Fig. 8. The trends and the amplitudes agree well, considering the uncertainties in the experiment as well as in the simulation. The results are also compared with analytical predictions in Fig. 8. The ratio T_{conv}/T_{ideal} is shown by the green line; T_{conv} is the calculated thrust for a convergent nozzle. Both T_{ideal} and T_{conv} assume top-hat exit velocity profile with zero boundary layer thickness. Whereas T_{ideal} assumes full expansion of the flow T_{conv} accounts for the unbalanced pressure at the nozzle exit, in supersonic conditions. The ratio is unity in subsonic conditions (NPR < 1.89) and it decreases with increasing NPR in supersonic conditions due to underexpansion. The solid light blue curve is the correlation CT for ASME nozzles from Ref. [9]; (recall earlier discussion that CT=Tac/ T_{ideal}). Its difference from the green curve is primarily due to boundary layer losses. Ideally, the experimental and CFD results should agree with the light blue (CT) curve. Differences seen are not unexpected. Apart from data uncertainty there can be differences in the boundary layer states. (There is considerable scatter in the data from which the correlation equations were derived in [9]). Thus, the agreement with the predictions is considered reasonable and these results, in fact, provided confidence in the present methods. The insert on the right of Fig. 8 is a sample CFD data clip of Mach number distribution that also shows the geometry of the *D*=1.3" ASME nozzle.

A sample CFD result with parametric variation is shown next. Figure 9 shows the effect of axial location of the (P16) plug crown as compared to experimental results. The plug is placed with $\triangle$x= -0.035" in the baseline case (extension E1, dark blue wall in the sketch on the side). Lip extensions are used to vary the relative location of the crown. Cases with extensions E2, E3 and E4 are shown by the red, green, and grey walls, respectively. The same color code is used for the data in Fig. 9, where the solid lines represent experimental data, and the dashed lines represent CFD results. It is seen that the data trends as well as amplitudes agree quite well between the experiment and CFD. These results provide added confidence and the adopted CFD procedure is deemed robust enough for further exploration of the effect of other factors for the problem at hand that has a huge parameter space.

Finally, a set of far-field noise data is shown in Fig. 10 for the P38, P39 and P40 plugs. Data at a low and a high NPR (1.89 and 4.3 corresponding M_J's of 1 and 1.4) are shown in Figs. 10(a) and 10(b), respectively. An inverse correspondence with the CFG data of Fig. 5 can be discerned. At low NPR, noise for LTO optimized case (P38, red curve) is low while the cruise optimized case has high noise. Thus, here a better thrust performance of the P38 case is accompanied also by lower noise. The situation is reversed at the high NPR where the cruise optimized case (P39, blue curve) has least noise (and high CFG). However, at the higher NPR there is screech that makes the comparisons difficult. These results will be examined carefully before the proposed paper is due. Finally, note that the compromise case (P40, green line) closely follows the LTO optimized P38 case in noise as well as CFG, making it a viable candidate for consideration in the larger NASA program.

Further experiments on noise as well as schlieren flow visualization will be conducted, especially addressing the effect of the porous plugs. More numerical simulations are ongoing. All results are to be summarized in the proposed paper.

Acknowledgement

The work is supported by NASA's Commercial Supersonic Technology (CST) Project under NASA's Advanced Air Vehicles Program.

References

1. Zaman, K.B.M.Q., Fagan, A.F., Bridges, J.E. and Heberling, B.C., 2022, "Flow and noise from supersonic plug nozzles", *AIAA Paper* 2022-2828, 28th AIAA/CEAS Aeroacoustics 2022 Conference, Southampton, UK, June 14-17, 2022.

2. Zaman, K.B.M.Q. and Heberling, B.C., 2021, "A study of flow and noise from supersonic plug nozzles", *AIAA Paper* 2021-2304, Aviation Forum, August 2-6, 2021.

3. Krull, H. G. and Beale, W. T., "Effect of Plug Design on Performance Characteristics of Convergent-Plug Exhaust Nozzles", *NACA RM* E54HO5, 1954.

4. Georgiadis, N.J., DalBello, T.W., Trefny, C.J., and Johns, A. L., "Aerodynamic Design and Analysis of High Performance Nozzles for Mach 4 Accelerator Vehicles", *AIAA Paper* 2006-16, 44th AIAA Aerospace Sciences Meeting and Exhibit, Reno, Nevada, 2006.

5. Angelino, G., "Approximate Method for Plug Nozzle Design", *AIAA J.*, vol. 2 (no. 7), pp. 1834-1835, 1964.

6. Hagemann, G., Immich, H., and Terhardt, M., "Flow Phenomena in Advanced Rocket Nozzles – The Plug Nozzle," *AIAA Paper* 98-3522, 34th Joint Propulsion Conference and Exhibit, Cleveland, OH, July 1998.

7. Korth, J.H., "Optimization of Plug Nozzles Using CFD Informed Design Space Querying", *AIAA Paper* 2023-xxxx, SciTech Conference, Orlando, FL, January 8-12, 2023.

8. Shapiro, A.H., "The dynamics and thermodynamics of compressible fluid flow, volume I", The Ronald Press Company, New York, USA, 1953.

9. Mikkelsen, K. L. and Brasket, R. G., "An Equation Set for ASME Nozzle Discharge and Thrust Coefficients," *AIAA Paper* 2011-1265, Jan. 2011.

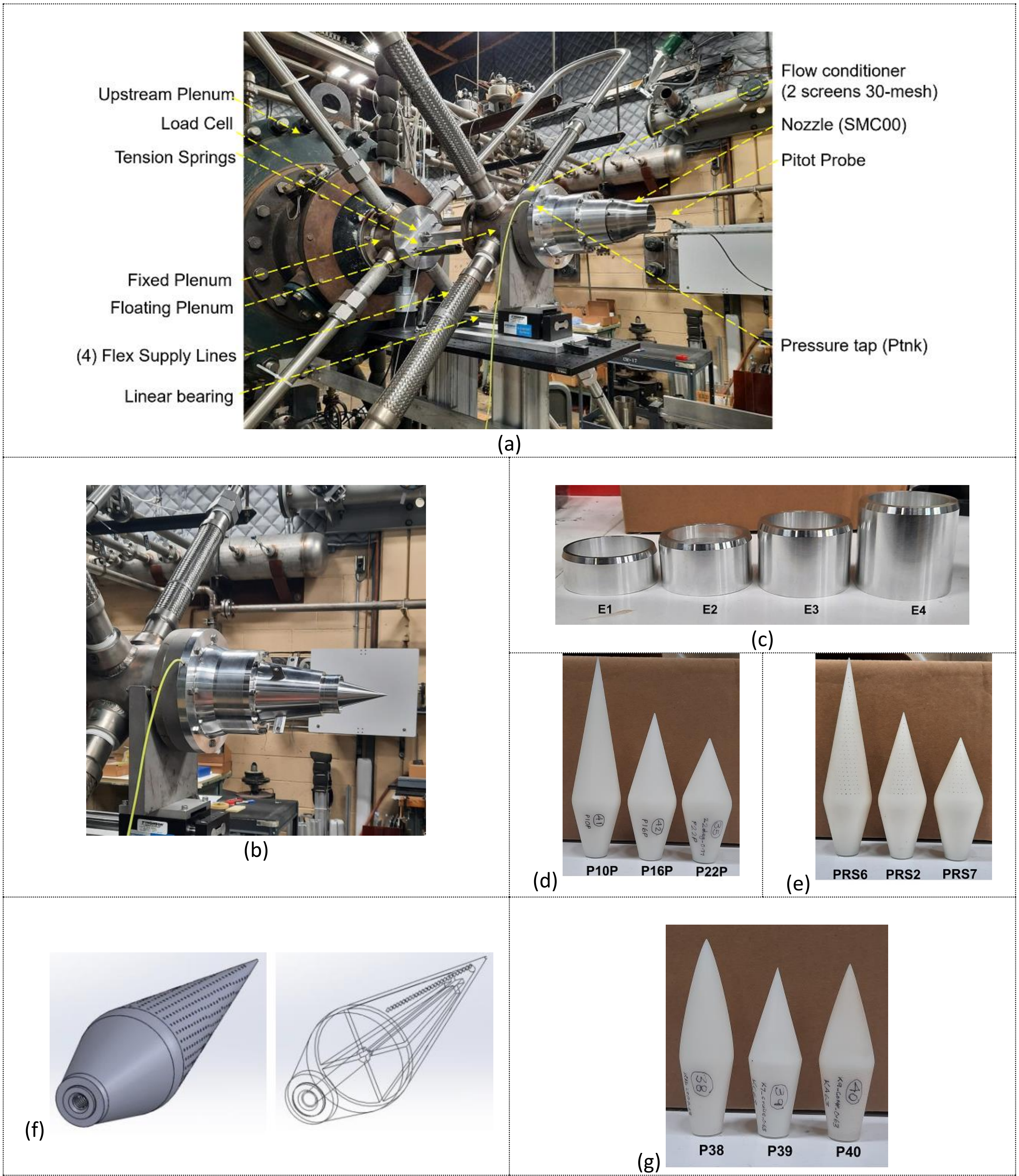

Fig. 1 Experimental Facility. (a) Thrust measurement setup, (b) Picture of plug nozzle on thrust stand, (c) picture of lip extensions (d) solid plugs, (e) porous plugs, (f) CAD drawing of a porous plug, (g) Optimized plugs via numerical study,

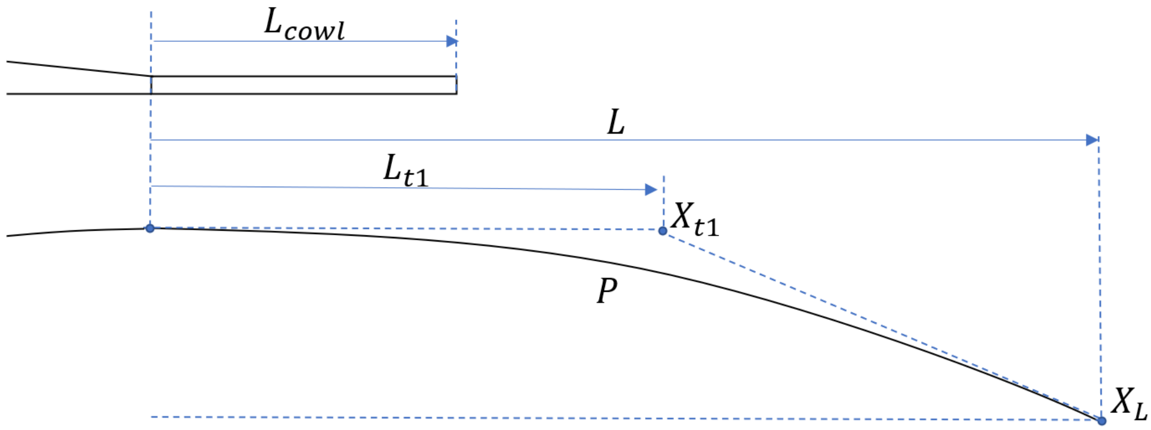

(a)

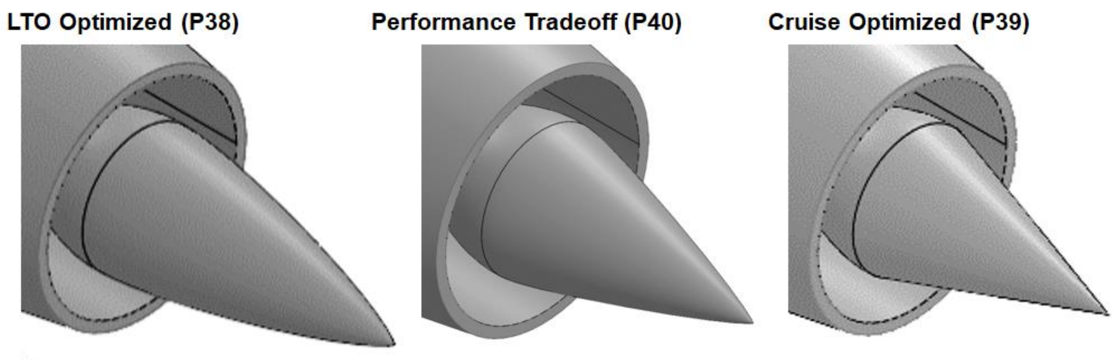

(b)

Fig. 2 Optimization of plug geometry via numerical simulation. (a) plug parameters varied for optimization, (b) Resultant plug geometries optimized for LTO (on left) and cruise (on right) conditions, as well as a 'compromise' geometry (in the middle).

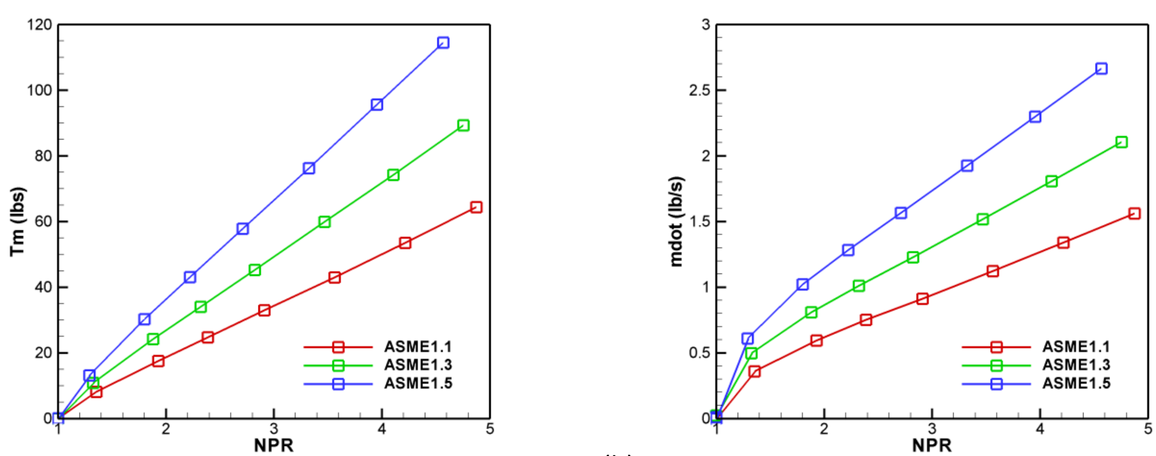

(a) (b)

Fig. 3 Calibration data with three 'ASME' nozzles having diameters of 1.1", 1.3" and 1.5". (a) Measured axial force (Tm), (b) measured mass flow rate (mdot), shown as a function of NPR.

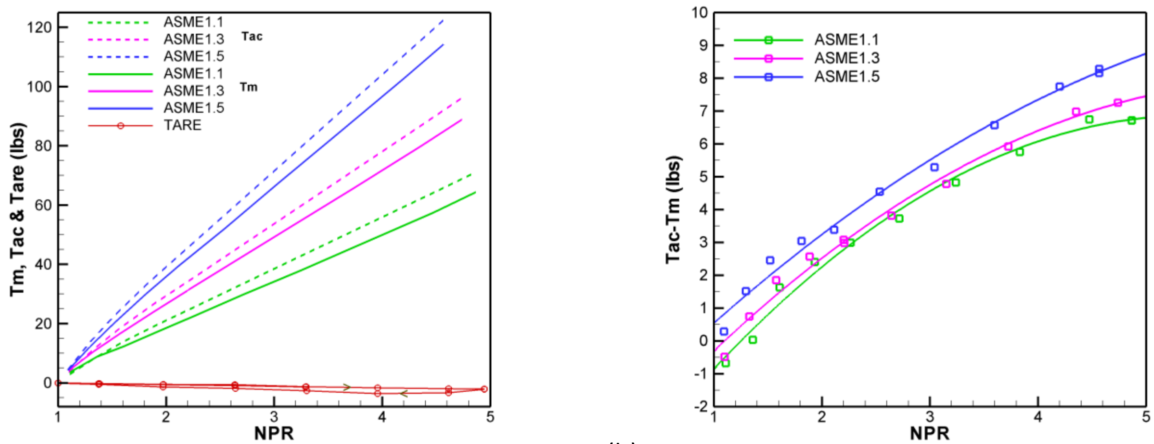

(a) (b)

Fig. 4 Force data for the three ASME nozzles. (a) Measured axial force (Tm) and corresponding calculated actual force (Tac) shown by the dashed and solid lines, respectively; also shown are 'tare' forces without flow by the red lines. (b) Corresponding difference (Tac-Tm) for the three nozzles.

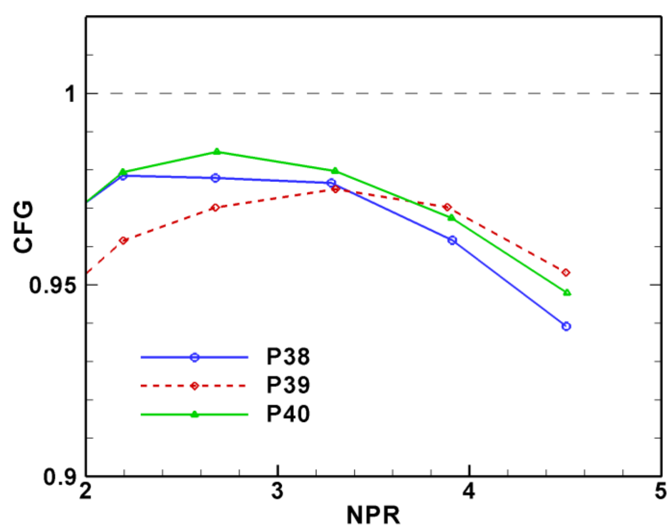

Fig. 5 Thrust coefficient vs. NPR for the three numerically optimized plugs (Fig. 2).

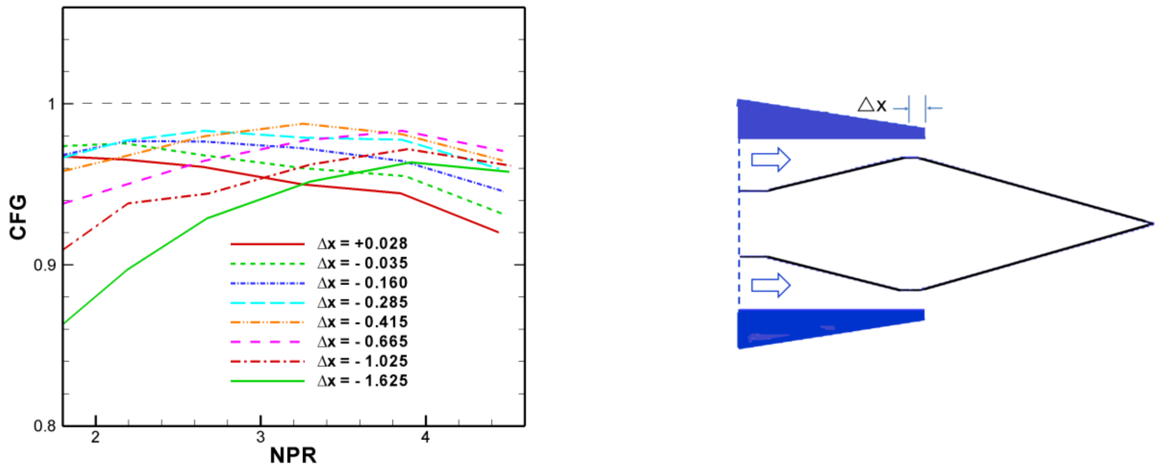

Fig. 6 Thrust coefficient vs. NPR for P40 plug for various crown location.

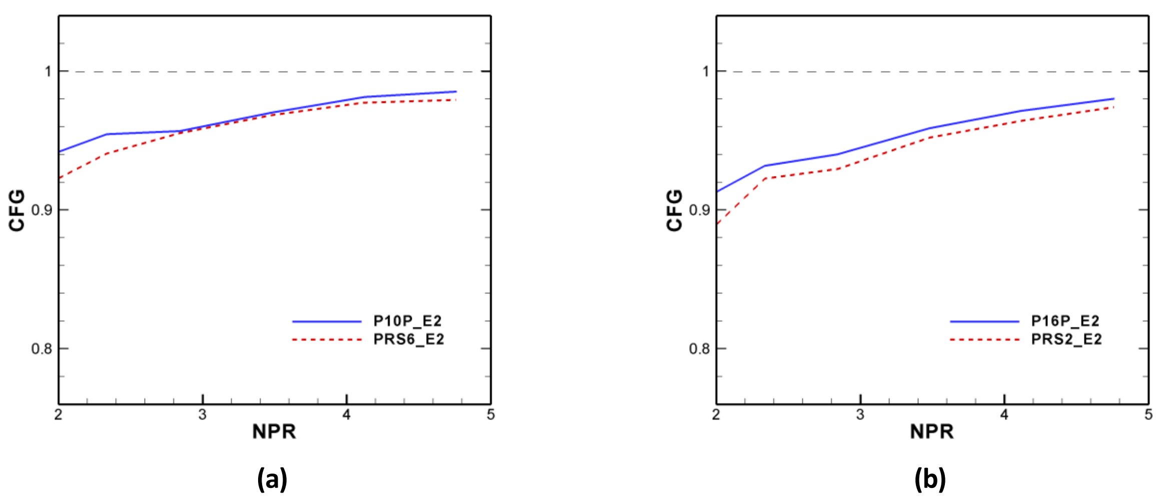

Fig. 7 Thrust coefficient vs. NPR showing plug porosity effect. Solid lines are for solid plugs while dashed lines are corresponding porous plugs. (a) 10° conic case (P10P vs PRS6), (b) 16° conic case (P16P vs PRS2).

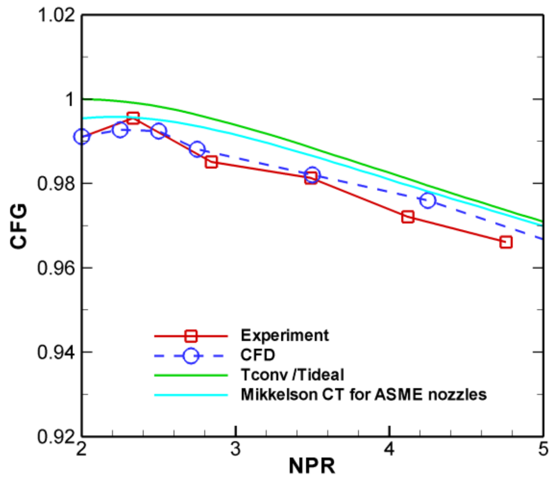

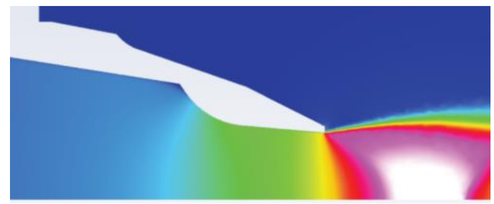

The nozzle geometry and typical CFD result showing Mach number contours.

Fig. 8 Thrust coefficient vs. NPR for the D=1.3" ASME nozzle. Red curve shows experimental data, blue dashed curve shows corresponding CFD prediction. Analytical prediction (zero BL thickness) is shown by the green curve while the light blue curve is a correlation for ASME nozzles from Ref. [8].

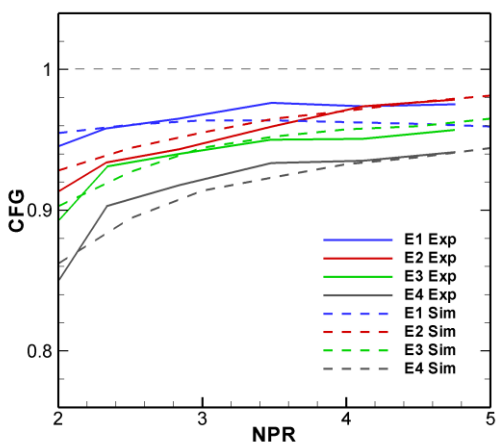

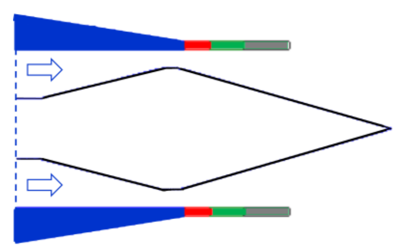

Fig. 9 Thrust coefficient vs. NPR for 16° conic plug with four lip extensions. Solid lines are experimental results while the dashed lines are CFD results

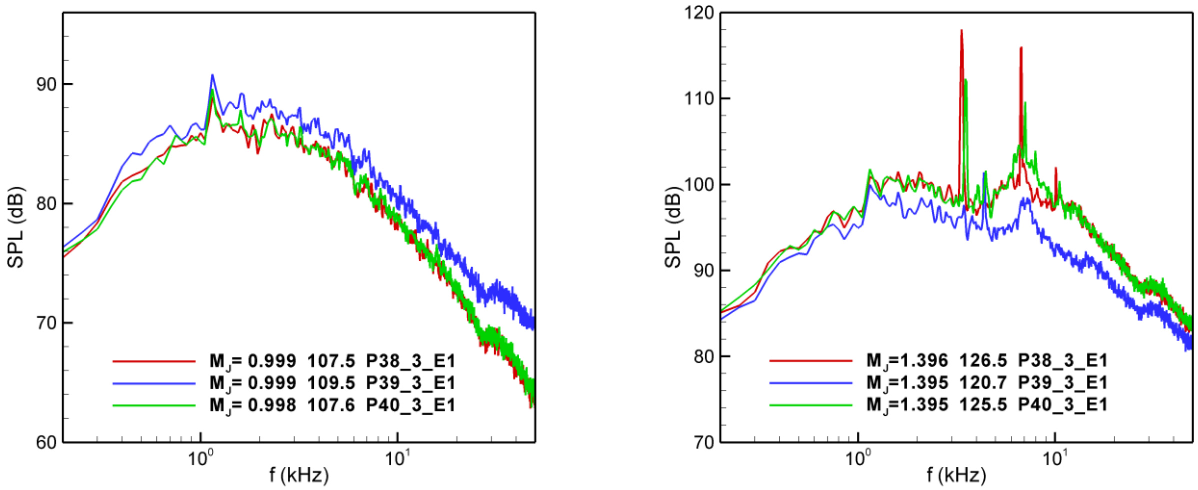

(a) **(b)**

Fig. 10 SPL spectra for the three plugs of Fig. 1(f) and Fig. 2; plug crown at x= -0.35. (a) M_J=1.00, (b) M_J =1.40.